Impurity-induced infrared spectra of CsBr. A breathing-shell model calculation

M. S. Haque* and D. Strauch
Institut für Theoretische Physik, Universität Regensburg, 8400 Regensburg, Federal Republic of Germany
(Received 7 February 1977)

The impurity-induced infrared spectra of CsBr doped with dilute concentrations of Tl^+, Rb^+, K^+, and Na^+ are calculated within the framework of a full breathing-shell-model formalism. Polarizability effects are consistently incorporated in the calculations, and these effects are shown to have significant influence on the calculated spectra of all the systems that are considered. For CsBr:Tl^+, perturbation of the defect's second-neighbor displacements are found to be essential for reproducing the observed spectra. The calculated spectra for all systems are in very good agreement with the corresponding observed ones.

I. INTRODUCTION

The impurity-induced infrared absorption spectra of CsBr and CsI have been measured[1,2] for a variety of isoelectronic defects. Among the many interesting features exhibited by these spectra are the low-frequency resonance-band modes (RBM) which appear in the Tl^+- and In^+-doped samples. The relatively large frequency shift and rapid broadening of the RBM line with increasing temperatures[1,3] in the Tl^+-doped crystals indicate strong anharmonicities in the vicinity of the defect. Moreover, contrary to normal expectations, the RBM frequency shifts to higher values with increasing temperatures. These effects, interesting as they are, remain uninvestigated and unexplained. However, in order to tackle the anharmonic problem it is absolutely essential to obtain a fairly reliable harmonic or "quasiharmonic" model for the perturbed crystal at a definite temperature, and this is the primary aim of the present theoretical investigations.

It is an established fact that in ionic crystals such as the Cs halides, the inclusion of polarization effects is essential for determining the dispersion of phonons correctly. Nevertheless, most of the theoretical investigations of the spectra of perturbed crystals use a formal force-constant (rigid-ion) model (without such polarization effects) in which the unperturbed phonons are calculated by means of one or another of the existing models which do include polarizability effects. Such an approach suffers from two important consequences. First, polarization effects are inconsistently and only partially accounted for, and this may result in serious errors if the polarizability of the defect ion is significantly different from that of the replaced host-crystal ion as is the case for the Tl^+ defect. Second, the formal force-constant model for the perturbed crystal is valid only for a particular symmetry. For example, in crystals in which every atom is at a center of inversion as is the case for the Cs halides, the infrared-active phonons are of symmetry type T_{1u}. Consequently, any formal force-constant model constructed by a fit to an observed infrared spectrum (of symmetry type T_{1u}) need not necessarily be valid for phonons of any other symmetry type such as A_{1g}, E_g, etc. In order to calculate the anharmonic properties of the infrared-active RBM it is not sufficient to know the perturbed harmonic phonons for the infrared-active symmetry type T_{1u} only, because the multiphonon vertices couple phonons of different symmetry types. The calculations described in this paper obtain a harmonic model for the perturbed crystal which is consistent for phonons of all symmetry types.

Consistent breathing-shell-model (BSM) calculations[4] of the U-center local-mode absorption have revealed only a weak effect of charge changes on the local-mode frequency, because the U center, at the local-mode frequency, vibrates essentially in a static surrounding. In low-frequency resonances, however, there is appreciable participation of the defect's neighbors in the vibrations,[5] and consequently charge changes may influence the RBM frequency significantly. This is another reason for the present investigation.

In this paper we present the calculations of the impurity-induced infrared absorption spectra for CsBr doped with dilute concentrations of Tl^+, K^+, Rb^+, and Na^+. The breathing-shell model (BSM) is used to calculate the unperturbed phonons for CsBr. For the perturbed-phonon calculations the Lifshitz technique in the BSM formalism[4] is applied. Standard Green's-function techniques are used to calculate the susceptibility and the impurity-induced absorption in a shell-model treatment.[6] The perturbed BSM parameters are adjusted to obtain the best possible fit to the experimental spectra of Ref. 2. This method offers two advantages. First, we are able to obtain a set of perturbed BSM parameters rather than a set of perturbed formal force constants. Consequently our resultant

model for the perturbed crystal should be symmetry independent. Second, polarization effects are included in a consistent manner both in the perturbed phonon dynamics and in the perturbed dipole moments.

We chose CsBr:Tl^+ for the investigation of the RBM problem, because the experimental spectrum for this system has more features in it than for the other systems, consequently allowing a more complete determination of the perturbed parameters. The only other calculation of the infrared spectra for this system is that of Ram and Agrawal[7] who use a formal force-constant model. Moreover, the agreement between the results of these calculations and experiments is not particularly satisfactory at higher frequencies.

The spectra of CsBr doped with K^+, Rb^+, and Na^+ are calculated primarily as a check on the reliability of our calculations. For these systems as well we shall demonstrate the importance of polarization effects and attempt to explain the origin of the experimental features.

II. THEORY

A. Dielectric susceptibility

The notation used in this section closely follows that of Refs. 4 and 6. The expression for the dielectric susceptibility tensor is given by

$$\chi_{\alpha\beta}(\omega) = (e^2/V)\,\underline{u}_\alpha^T(\underline{Z}_0 + \Delta\underline{Z}) \times (\underline{G}_0 - \underline{G}_0\underline{T}\underline{G}_0)(\underline{Z}_0 + \Delta\underline{Z})\,\underline{u}_\beta . \quad (1)$$

The corresponding expression in Ref. 6 misses the frequency-independent contributions. Here V is the crystal volume and u is the polarization unit vector of the external electric field. The matrices $\underline{Z}_0$ and $\Delta\underline{Z}$ contain the unperturbed charges and the charge perturbations, respectively, in units of the elementary charge e. The Green's-function matrix of the unperturbed crystal is denoted by $\underline{G}_0$, and the matrix $\underline{T}$ is the t matrix, which accounts for the perturbed phonon dynamics. In real-space representation the elements of these matrices will be denoted by a Cartesian index $\alpha = x, y, z$; a sublattice index κ; a cell index $l = 1, \ldots, N$; and the type of degree of freedom $P = C, S, B, E$. Here C refers to the core, S refers to the (dipole) displacements of the shells, B refers to the (monopole) breathing displacements, and E refers to the electric field.

The expression for the susceptibility tensor in the low-concentration single-site scattering approximation up to terms linear in the concentration p is given by

$$\chi_{\alpha\beta}(\omega) = (e^2N/V)\,\underline{u}_\alpha^T[\underline{\zeta}_0\underline{\gamma}_0(0)\underline{\zeta}_0 + p\underline{X}]\,\underline{u}_\beta . \quad (2)$$

The first term represents the host-lattice susceptibility, and the second term represents the defect-induced modification

$$\underline{X} = -\underline{\zeta}_0\underline{\gamma}_0(0)\underline{t}\,\underline{\gamma}_0(0)\underline{\zeta}_0 + \underline{\zeta}_0\underline{\gamma}_0(0)(\underline{1} - \underline{t}\,\underline{g}_0)\Delta\underline{Z} + \Delta\underline{Z}(\underline{1} - \underline{g}_0\underline{t})\underline{\gamma}_0(0)\underline{\zeta}_0 + \Delta\underline{Z}(\underline{g}_0 - \underline{g}_0\underline{t}\,\underline{g}_0)\Delta\underline{Z} . \quad (3)$$

Here $\Delta\underline{Z}$, $\underline{t}$, and $\underline{g}_0$ represent the charge perturbation matrix, the t matrix, and the unperturbed Green's-function matrix, respectively, for a single defect with

$$\underline{t} = \underline{\lambda}(\underline{1} + \underline{g}_0\underline{\lambda})^{-1} ,$$

where λ is the perturbation matrix for a single defect. The quantities $\underline{\zeta}_0$ and $\underline{\gamma}_0(\vec{q})$ are defined by

$$Z_0(l\kappa\alpha P, l'\kappa'\alpha'P') = \zeta_0(\kappa P)\delta_{l,l'}\delta_{\kappa,\kappa'}\delta_{\alpha,\alpha'}\delta_{P,P'}$$

and

$$G_0(l\kappa\alpha P, l'\kappa'\alpha'P') = N^{-1}\sum_{\vec{q}} \gamma_0(\kappa\alpha P, \kappa'\alpha'P' \mid \vec{q}) \times \exp[i\vec{q}\cdot(\vec{R}_{l\kappa} - \vec{R}_{l'\kappa'})] .$$

The translational symmetry of Z_0 makes all contributions in Eqs. (2) and (3) vanish except those for $\vec{q}$ equal to zero; then one has, for example,

$$(\underline{u}_\beta^T\underline{Z}_0\underline{G}_0)_{l\kappa\alpha P} = \sum_{\kappa'P'} \zeta_0(\kappa'P')\,\gamma_0(\kappa'\alpha P', \kappa\alpha P \mid \vec{q}=0) . \quad (4)$$

Application of group theory further reduces the problem, and this reduction is accomplished by means of unitary transformations constructed from symmetry basis vectors $\underline{\xi}(\Gamma rs) = \{\xi(\Gamma rs \mid l\kappa\alpha)\}$. Here r and s refer to the rth partner and the sth realization of a given irreducible representation Γ. Thus the matrices appearing in Eq. (3) can be expressed either in the $(l\kappa\alpha P)$ or in the (ΓrsP) representation.

In the symmetrized representation,

$$\underline{X} = \sum_{\Gamma r} \underline{X}(\Gamma r) ,$$

where a typical transformation to the symmetrized representation is given by

$$g_0(\Gamma rsPs'P') = \sum_{l\kappa\alpha}\sum_{l'\kappa'\alpha'} \xi(\Gamma rs \mid l\kappa\alpha) \times g_0(l\kappa\alpha P, l'\kappa'\alpha'P')\,\xi(\Gamma rs' \mid l'\kappa'\alpha'P') .$$

B. Model for the perturbed crystal

For crystals of Cs-halide structure the point-symmetry group is O_h. The electric field unit vector transforms according to the irreducible representation T_{1u}, which is therefore the only one needed for calculating the susceptibility. Additionally we shall assume linear polarization along the

x axis, and consequently we need to consider only that partner of the T_{1u} irreducible representation which is polarized along the x direction.

We choose the origin of the coordinate system to be at the defect site. The first-, second-, and fourth-nearest neighbors are then situated at $\langle 111\rangle$, $\langle 200\rangle$, $\langle 222\rangle$, and equivalent positions, respectively.

The influence of defect-induced changes of the following breathing-shell-model (BSM) parameters are investigated: (i) change in mass at defect site, which is denoted by $\delta M = M_d - M_0$, where M_d and M_0 are the defect mass and the host-crystal ion mass, respectively; (ii) change in longitudinal and transverse shell-shell force constants between the defect and the first neighbors, denoted by δf_l and δf_t, respectively; (iii) change in shell and core charge at defect site, given by δY and $-\delta Y$, respectively, implying zero change in ionic charge; (iv) change in the isotropic core-shell force constant at the defect site δG. The changes δY and δG account for the change in the polarizability. This set of parameters will turn out to be insufficient to describe the Tl^+-induced spectrum. Therefore the effect of a possible lattice relaxation around the defect is to be investigated since it has been found to be important in other cases[8]; this requires the study of the following changes: (v) change in longitudinal shell-shell force constant between neighboring first and fourth neighbors δf_4; (vi) change in the longitudinal shell-shell force constant between neighboring first and second neighbors δf_s; (vii) change in the longitudinal shell-shell force constant between two neighboring first neighbors δf_1. Even then the calculation of the Tl^+-induced spectrum lacks satisfactory agreement. Because of the relative closeness of the second neighbors we investigate finally the (viii) change in the longitudinal shell-shell force constant between the defect and the second neighbors δf_2.

For the host crystal, the transverse force constant is about an order of magnitude smaller than the longitudinal, and we have assumed a similar relation for the perturbed case; therefore the transverse force-constant perturbations have been generally neglected. All perturbed parameters except δM are to be considered adjustable.

Eleven different degrees of freedom (realizations) in the T_{1u} symmetry are affected by these nine different perturbed parameters. These, along with their normalized basis vectors for the irreducible representation T_{1u} are given in Table I. The latter can be found in the article by Dettmann and Ludwig.[9] In Table I, the subscripts C, S, B, E refer to core, shell, breathing, and electric field degrees of freedom, respectively. The superscripts l and t refer to longitudinal and transverse basis vectors, respectively. The numbers 0, 1, 2, 4 associated with ξ refer to defect, first, second, and fourth neighbors, respectively.

Using the symmetry basis vectors listed in Table I, the perturbation matrix in defect space expressed in symmetry coordinates is shown in Table II.

Using the formalism described above we have calculated the frequency-dependent absorption constant defined by

$$K(\omega) = (4\pi\omega/cn)\ \mathrm{Im}\,\chi(\omega)\,, \tag{5}$$

where c is the velocity of light and n is the index of refraction which is assumed to be constant. For cubic crystals

$$\chi(\omega) = \frac{1}{3}\sum_{\alpha}\chi_{\alpha\alpha}(\omega)\,.$$

III. RESULTS AND DISCUSSION

All calculations which are described in this paper are valid for temperature 4.2 K. The unperturbed host-crystal phonons for CsBr at this temperature

TABLE I. Symmetry basis vectors for the irreducible representation T_{1u} $\underline{\xi}_p(-\vec{r}) = \underline{\xi}_p(\vec{r})$ for $P = C, S, E$; $\xi_B(-\vec{r}) = -\xi_B(\vec{r})$.

	000	222 111	−222 −111	−2 −22 −1 −11	2 −22 1 −11	200	020	002
$\vec{\xi}_C(0), \vec{\xi}_S(0), \vec{\xi}_E(0)$	100	000	000	000	000	000	000	000
$(24)^{1/2}\vec{\xi}^l_S(1), (24)^{1/2}\vec{\xi}^l_S(4)$	000	111	1 −1 −1	1 1 −1	1 −1 1	000	000	000
$(48)^{1/2}\vec{\xi}^t_S(1)$	000	2 −1 −1	211	2 −1 1	2 1 −1	000	000	000
$\sqrt{2}\,\vec{\xi}^l_S(2)$	000	000	000	000	000	100	000	000
$2\vec{\xi}^t_S(2)$	000	000	000	000	000	000	100	100
$(8)^{1/2}\xi_B(1), (8)^{1/2}\xi_B(4)$	0	−1	1	1	−1	0	0	0
$\sqrt{2}\,\xi_B(2)$	0	0	0	0	0	−1	0	0

TABLE II. Perturbation matrix $\underline{\lambda}(T_{1u})$ in symmetrized representation.

	$\xi_C(0)$	$\xi_S(0)$	$\xi_S^l(1)$	$\xi_S^t(1)$	$\xi_S^l(4)$	$\xi_S^l(4)$	$\xi_S^t(2)$	$\xi_B(1)$	$\xi_B(4)$	$\xi_B(2)$	$\xi_E(0)$
$\xi_C(0)$	$(\delta G - \omega^2 \delta M)$										
$\xi_S(0)$	$-\delta G$	λ_{22}									
$\xi_S^l(1)$	0	$(-4/\sqrt{6})\,\delta f_l$	λ_{33}								
$\xi_S^t(1)$	0	$(-4/\sqrt{3})\,\delta f_t$	$(-4/3\sqrt{2})\,\delta f_1$	λ_{44}							
$\xi_S^l(4)$	0	0	$-\delta f_4$	0	δf_4						
$\xi_S^l(2)$	0	$-\sqrt{2}\,\delta f_2$	$(2/3\sqrt{3})\,\delta f_s$	$(-4/3\sqrt{6})\,\delta f_s$	0	$\delta f_2 + \frac{4}{3}\delta f_s$					
$\xi_S^t(2)$	0	0	$(-4/3\sqrt{6})\,\delta f_s$	$(-4/3\sqrt{3})\,\delta f_s$	0	0	$\frac{4}{3}\delta f_s$				
$\xi_B(1)$	0	$(-4/\sqrt{6})\,\delta f_l$	λ_{83}	$(-2/\sqrt{6})\,\delta f_1$	δf_4	$(2/\sqrt{3})\,\delta f_s$	$(-4/\sqrt{6})\,\delta f_s$	λ_{88}			
$\xi_B(4)$	0	0	$-\delta f_4$	0	δf_4	0	0	δf_4	δf_4		
$\xi_B(2)$	0	$-\sqrt{2}\,\delta f_2$	$\frac{2}{3}\delta f_s$	$(-16/3\sqrt{2})\,\delta f_s$	0	$\delta f_2 + (4/\sqrt{3})\,\delta f_s$	0	$4\delta f_s$	0	$(\delta f_2 + 4\delta f_s)$	
$\xi_E(0)$	$-\delta Y$	δY	0	0	0	0	0	0	0	0	0

$$\lambda_{22} = \delta G + \tfrac{8}{3}(\delta f_l + 2\delta f_t) + 2\delta f_2$$

$$\lambda_{33} = \delta f_l + \delta f_4 + \tfrac{1}{3}\delta f_s + \tfrac{4}{3}\delta f_1$$

$$\lambda_{44} = \delta f_t + \tfrac{4}{3}\delta f_s + \tfrac{2}{3}\delta f_1$$

$$\lambda_{83} = \delta f_l - \delta f_4 + \delta f_s + (2/\sqrt{3})\,\delta f_1$$

$$\lambda_{88} = \delta f_l + \delta f_4 + 3\delta f_s + 2\delta f_1$$

TABLE III. BSM parameters (Ref. 10) for CsBr at 4.2 K. (Force constants in units of e^2N/V, charges in units of e.)

$A=2f_l$	$B=2f_t$	g_+	g_-	G_+	G_-	Y_+	Y_-	Z_+
11.18	−1.11	284.1	212.9	1142	143.4	−6.80	−2.78	1

were obtained from the BSM calculations of Mahler and Engelhardt.[10] The macroscopic parameters used in the phonon calculations are given in Ref. 10. We present here the BSM model parameters which are listed in Table III.

In Table III, f_l and f_t refer to the longitudinal and transverse shell-shell force constants between the nearest neighbors, $g_\pm$ refer to the core-shell springs for the breathing displacements, $G_\pm$ refer to the springs for the dipolar core-shell displacements, and $Y_\pm$ and $Z_\pm$ are the shell and ionic charges, respectively. In the following, charges, force constants, and polarizabilities are given in units of the elementary charge e, $e^2N/V=3032$ ergs/cm^2, and Å^{-3}, respectively.

A. Resonance frequency of CsBr:Tl$^+$

The experimental infrared spectrum for CsBr:Tl$^+$, which is shown in the lower half of Fig. 1, consists of a distinct resonance band mode (RBM) peak at $\omega_r=16.95$ cm^{-1} and some additional absorption on the low-frequency wing of the reststrahlen band ($\omega_{TO}=78.5$ cm^{-1}, cf. Ref. 10). No measured spectrum exists for frequencies higher than ~70 cm^{-1}.

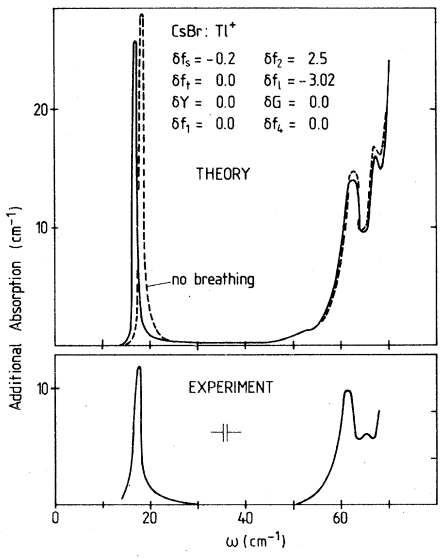

FIG. 1. Calculated and experimental (Ref. 2) infrared spectra of CsBr:Tl$^+$. Defect concentration $p=6.4\times10^{-2}$ mole%.

The resonance condition is given by

$$\mathrm{Re}\|\underline{1}+\underline{g}_0(T_{1u},\omega_r)\underline{\lambda}(T_{1u},\omega_r)\|=0\,. \tag{6}$$

The experimental value of ω_r in Eq. (6) is used to reduce the number of independent model parameters by one, and to simultaneously guarantee the correct frequency for the RBM in the calculated spectrum. As will be discussed below, different parameters influence different features of the spectrum.

Equation (6) establishes a relation between two perturbation parameters when the remaining parameters are kept constant. This is demonstrated in Figs. 2 and 3. All three curves presented in Fig. 2 show that the transverse coupling to the defect has to be enhanced when the longitudinal coupling is weakened and vice versa in order to hold the resonance frequency constant. Unlike the case of the U-center local mode[4] the curves shown in Fig. 2 deviate very strongly from a linear behavior, which indicates an appreciable participation of the defect's neighboring atoms in the resonance vibration. The straight line which is obtained for an Einstein oscillator (i.e., neglecting all but the defects motion) is also shown in the figure.

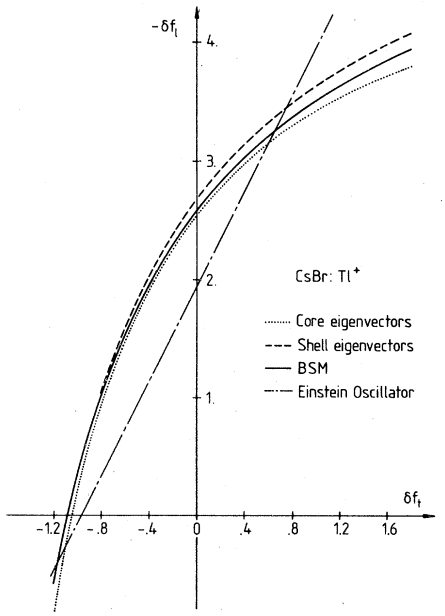

FIG. 2. Plot of δf_l vs δf_t obtained from the resonance condition using three different models.

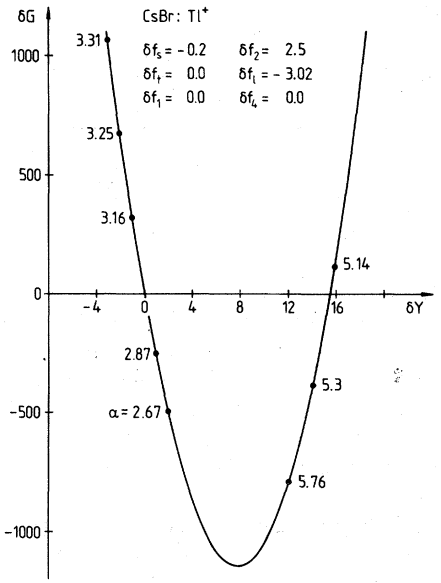

FIG. 3. Plot of $\delta\gamma$ vs δG obtained from the resonance condition. All other parameters are held constant at the values shown. Some values of the polarizability, Eq. (7), for points along the curve are shown.

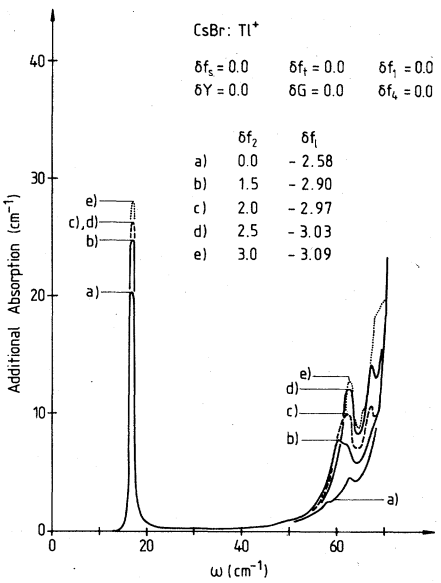

FIG. 4. Calculated infrared spectra of CsBr:Tl$^+$ for five different values of δf_2. The parameter δf_t is determined from the resonance condition. All other parameters are held constant at the values shown.

In Fig. 2, the effect of using a formal force-constant model is also indicated. Two such calculations are presented. In one the shell eigenvectors are used and in the other the core eigenvectors for calculating the unperturbed Green's-function matrix $\underline{g}_0$. The deviations of these curves from the consistent BSM calculation (solid line) reflect the effects of the relative core-shell displacements.

The sensitivity of the RBM frequency to δG and δY is shown in Fig. 3, in which Eq. (6) is used to calculate δG as a function of δY. The lowest value of δG is that for which the resultant core-shell spring constant is zero, i.e., negative values of the core-shell spring are not obtained. The polarizability of the defect, which is given by

$$\alpha = (Y_+ + \delta Y)^2/(G_+ + \delta G)\,, \tag{7}$$

varies along the curve as shown.

The RBM frequency is also found to be sensitive, although to a much smaller extent, to the parameters δf_1, δf_2, δf_3, and δf_4, which do not affect the defect directly, but act through the neighbors. The question as to which values of all these parameters represents the physical model of the crystal cannot be answered by the position of the RBM frequency alone. A more complete determination of the model for the perturbed crystal will be provided by the complete absorption spectrum to which we now turn.

B. One-phonon spectrum of CsBr:Tl$^+$

In addition to the RBM peak at 16.95 cm^{-1} the spectrum has two additional peaks at roughly 61 and 65 cm^{-1} (see Fig. 1). The last two are crucial features in determining our model. These two peaks cannot be reproduced within the framework of a nearest-neighbor model (see also Ref. 7), i.e., by means of the parameters δf_l, δf_t, δY, δG, which directly influence the defect motion, or by means of δf_1, δf_4, δf_s, which result from relaxation effects.

With the above-mentioned force-constant changes one can obtain the RBM peak and a small bump at 62.5 cm^{-1}, whose height along with that of the RBM peak can be raised or lowered without producing any qualitative changes in the spectra. The parameter δf_s produces a significant peak at 60.2 cm^{-1} for $-2.0 \lesssim \delta f_s \lesssim -1.0$, but fails to reproduce the peak at 65 cm^{-1}.

Moreover, any combination of the above-mentioned parameters fails to reproduce the peak at 65 cm^{-1} as well. We shall now demonstrate that within our model this peak can be obtained by a nonzero value of δf_2.

For the spectra shown in Fig. 4, δf_2 is varied, and δf_l is obtained by means of a fit to the RBM frequency. All other parameters are held constant at zero. Curve (a) in Fig. 4, for which $\delta f_2 = 0$, shows a small bump at 62.5 cm^{-1} and nothing at higher frequencies. As δf_2 is increased, this bump gathers intensity until it becomes a well-defined peak for $\delta f_2 = 2.0$ [curve (c)], and in addition a small peak appears at 67.4 cm^{-1}. As δf_2 is further increased, the peak at 62.5 cm^{-1} becomes sharper, and by $\delta f_2 = 3.0$ [curve (e)], the 67.5-cm^{-1} peak dis-

appears. These curves indicate a very strong coupling between the defect and the second neighbors, a very surprising result in view of the fact that the model for the unperturbed crystal does not contain such an interaction.

A calculated spectrum which we consider to be in good agreement with experiment is shown in the upper half of Fig. 1 (full line). The parameters which determine this spectrum are quoted in the figure. Starting from this set of parameters, the influence of the various parameters on the spectrum shall now be demonstrated in Figs. 5–7.

The spectra shown in Fig. 5 are obtained by varying δf_t for a fixed value of $\delta f_2 = 2.5$. The parameter δf_l is obtained from the resonance condition. Qualitative changes occur in the peak at 62.5 cm^{-1} as δf_t is varied, but the dramatic effect occurs in the 67.4-cm^{-1} peak. The latter disappears for $\delta f_t \gtrsim +0.2$.

Consider now the spectra shown in Fig. 6 in which δf_s is varied as the independent parameter for $\delta f_2 = 2.5$, and δf_l being obtained from the resonance condition. For the values of δf_s considered here, the effect on the spectra is quantitative in that the peak at 62 cm^{-1} gathers intensity as δf_s is decreased from 0.2 to −0.4. Otherwise the qualitative appearance remains unchanged. Variation of δf_1 and δf_4 leads to similar qualitative changes but does not lead to an as well-defined peak around 60 cm^{-1}.

Let us now turn our attention to the parameters which determine the change in polarizability of the

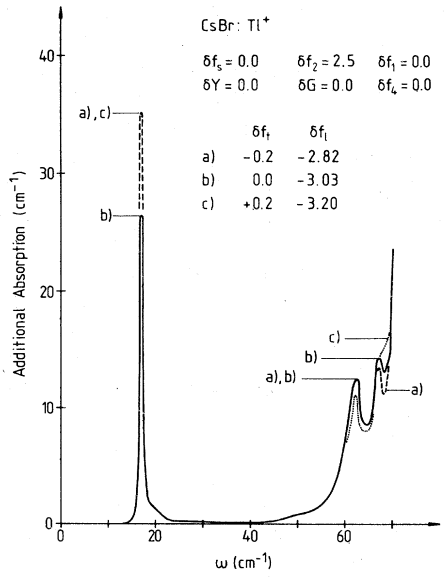

FIG. 5. Calculated infrared spectra of CsBr:Tl^+ for three different values of δf_t. The parameter δf_l is determined from the resonance condition. All other parameters are held constant at the values shown.

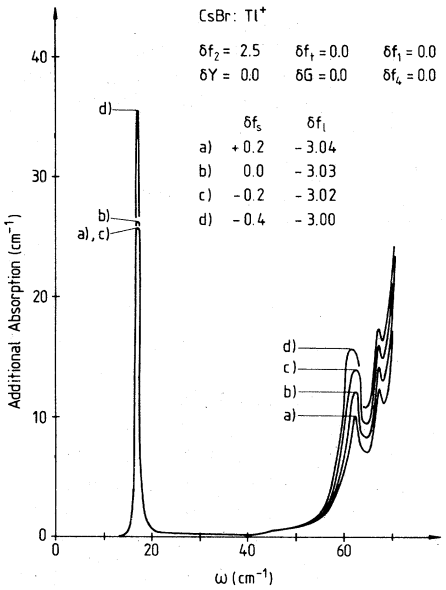

FIG. 6. Calculated infrared spectra of CsBr:Tl^+ for four different values of δf_s. The parameter δf_l is determined from resonance condition. All other parameters are held constant at the values shown.

defect, i.e., δY and δG. Figure 7 shows three spectra which are calculated with parameters that are picked off the curve shown in Fig. 3.

Recall that in Eq. (3) the contribution to the defect-induced susceptibility is separated into four terms from which the last three terms have nonzero contributions only for nonzero values of δY. For convenience let us denote these four different

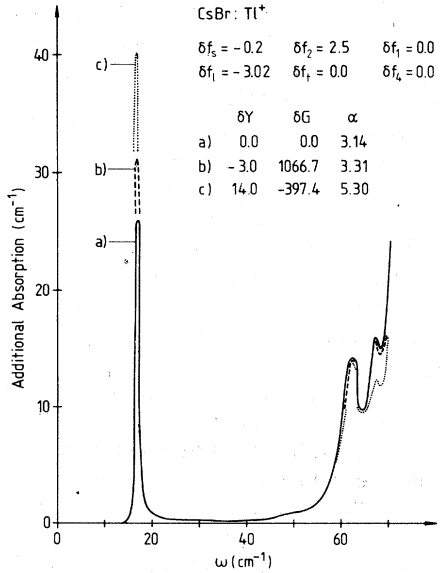

FIG. 7. Calculated infrared spectra for three different values of defect polarizability. Perturbed parameters are obtained from Fig. 3.

contributions by χ_1, χ_2, χ_3, and χ_4, respectively. For $\delta Y = -3$, i.e., curve (b) in Fig. 7, $\chi_2 + \chi_3$ is an order of magnitude smaller and χ_4 three orders of magnitude smaller than χ_1. For $\delta Y = 14$, i.e., curve (c), the dipole moment of the Tl^+ ion ($\alpha = 5.3$) is much larger than that of the Cs^+ ion[11] ($\alpha = 3.14$), and hence χ_2, χ_3, and χ_4 are expected to have relatively larger contributions near the RBM peak. This is precisely what is found. Near the resonance frequency $\chi_2 + \chi_3 \sim 0.9\chi_1$, and $\chi_4 \sim 0.1\chi_1$. At higher frequencies the contributions from χ_2, χ_3, and χ_4 are an order of magnitude smaller than that from χ_1.

The intensity of the RBM peak is expected to increase with increasing polarizability. Despite computational uncertainties the curves in Fig. 7 tend to confirm this. The peak at 62.5 cm^{-1} is not particularly affected by changes in α, but for $\alpha = 5.3$, the 67.4-cm^{-1} peak is pushed down below the neighboring peak in accordance with experiment (see Fig. 1). It is interesting to note that the polarizability of Tl^+ in TlBr is 5.1,[11] which is very close to the value appropriate to curve (c). However, singly ionized thallium is a highly polarizable ion whose polarizability depends very strongly on its environment.[11] Hence it is not at all certain that the polarizability of Tl^+ in TlBr should be appropriate for a substitutional Tl^+ ion in CsBr. Also, the height of the RBM peak relative to those of the high-frequency peaks is far too large and therefore in serious disagreement with experiment. Although some of this discrepancy in the peak heights can be reduced by the inclusion of defect-induced anharmonic effects which are known to be strong for this system,[3] it is unlikely that anharmonicities alone can resolve such a large discrepancy. Note also that the value of δY appropriate to curve (c) is 14.0, which indicates a rather large positive shell charge for Tl^+, namely $Y(Tl^+) = +7.2$. This fact is difficult to explain on physical grounds. To conclude the discussion on the effects of polarizability changes, it appears that although the RBM frequency is very sensitive to changes in the shell charge and the core-shell spring constant, no such changes are warranted on the basis of best overall agreement with the experimental spectra for CsBr:Tl^+.

Let us now return to Fig. 1 where we present that spectrum which we consider to be our best result and compare it with the experimental result. Although the overall agreement between the experimental and calculated results is good, there are certain discrepancies which require discussion.

First, the overall absorption in the calculated spectrum is too large, roughly by a factor of 2. This might be accounted for by possible errors in the value of the concentration for which we have used the one quoted in Ref. 2, namely $p = 6.4 \times 10^{-2}$ mole%. If instead of the above we use $p = 4.1 \times 10^{-2}$ mole%, the 62.5-cm^{-1} peak comes in perfect agreement with experiment, and the integrated RBM absorption agrees to within 10%. A similar disagreement in the line intensity in CsI:Tl^+ was encountered by Martin.[12] Note that the half width of the calculated RBM peak is ~1.1 cm^{-1}, whereas the experimental value is 1.5 cm^{-1}. The disagreement in height and width for the RBM peak must be due to anharmonic effects.

The second important discrepancy between theory and experiment lies in the frequencies of the two peaks at higher frequencies. We believe that these two peaks result from defect-activated host-crystal phonons, since their absolute positions are independent of the perturbation parameters, as we have demonstrated in Figs. 4–7. Hence the small discrepancies in the frequencies of these peaks from their corresponding experimental values reflect uncertainties in the calculated host-crystal BSM phonons. This error, which is relatively small, has a very significant consequence on the appearance of the small peak at 67.4 cm^{-1}, in the calculated spectrum. The frequency of the corresponding experimental peak is roughly 65 cm^{-1}. This difference pushes the calculated peak a little farther on the rapid rise towards the reststrahlen frequency, and thus gives it the peculiar appearance.

In Fig. 1 we also demonstrate the effect of the breathing degree of freedom on the calculated spectrum. The spectrum drawn in broken line is one in which the breathing coordinates on the first neighbors are set equal to zero. This has the effect of stiffening the effective springs between the defect and its first neighbors. Consequently the resonance frequency shifts upwards.

The breathing effect, although not large, is also significant for the two peaks at higher frequencies. The breathing coordinates on the second and fourth neighbors do not play a significant role, and their effect is not visible on the scale of the graph presented. There are two reasons for this. One factor is the distance of these ions from the defect site. The other is the fact that these ions are the Cs^+ ions, which are less polarizable than the nearest-neighboring Br^- ions.[11]

C. CsBr:Rb^+, K^+, Na^+

Unlike Tl^+ which, on account of its two 6s electrons in the outer shell, has a large polarizability which is strongly volume-dependent, Rb^+, K^+, and Na^+ have inert gas structures and consequently possess polarizabilities which do not significantly vary with volume. Moreover their ionic polariz-

TABLE IV. Parameters for Rb^+, K^+, and Na^+ in CsBr.

Impurity	α	p (10^{-2} mole%)	Model	δf_1 (e^2N/V)	δG (e^2N/V)	$\delta Y(e)$
Rb^+	1.79[a]	5.0	I	−2.1	816	0
			II	−2.1	0	1.6
			III	−1.8	0	0
K^+	1.201[a]	9.5[b]	I	−2.5	1787	0
			II	−2.5	0	2.6
			III	−2.0	0	0
Na^+	0.255[a]	1.1[b]	I	−2.7	12 650	0
			II	−2.7	0	4.8
			III	−2.0	0	0

[a]Reference 11. [b]Reference 2.

abilities are considerably smaller than that of Cs^+ in CsBr. These considerations are taken into account in our calculations.

For these systems, three different model calculations are performed. The parameters are listed in Table IV. In model I, δG is adjusted to obtain the desired value of the polarizabilities, which are also listed in Table IV. In model II, the same effect is obtained by adjusting the value of δY, and in model III no polarizability changes are included in the calculations.

The only other parameter in these calculations is δf_1 which is adjusted to obtain the best agreement with experiment. Inclusion of δf_t requires different values for δf_1 without any qualitative changes in the spectral features. All the remaining parameters are set equal to zero in these calculations.

The spectra calculated with the model-I parameters are shown in Fig. 8, in which we also reproduce the experimental results of Ref. 2 for comparison. Model II reproduces exactly the same spectra for Rb^+ and Na^+, with only a small difference in height for the large peak in the K^+ spectrum. The spectra obtained with the model-III parameters are similar. Note that δf_1 has exactly the same value in model I and model II, in which the correct ionic polarizabilities of the defects are accounted for, but have different values in model III, where the ionic polarizabilities of the defects are the same as that for Cs^+. Also one expects a continuous decrease of δf_1 with decreasing defect size which is found in model I and model II, but only partially in model III. We present these facts as evidence for the importance of incorporating polarizability changes in defect calculations.

The correspondence between the calculated and the experimental spectra, as shown in Fig. 8, is striking. The values for defect concentrations used are listed in Table IV. For the K^+ and Na^+ systems, these values correspond to the experimental ones.[2] For the Rb^+ system no experimentally determined value is available, but $p = 5.0 \times 10^{-2}$ mole% gives the best agreement between the calculated and experimental spectrum.

The only serious discrepancy between the calculated and the experimental spectra is in the frequencies of the calculated peaks which lie approximately 5 cm^{-1} below the experimentally measured peaks. These peaks can be moved continuously backwards or forwards in frequency by adjusting δf_1. This effect is demonstrated in Fig. 9 for CsBr:K^+. Note that the intensities of the peaks gradually decrease as they shift towards higher frequencies; and that for a given value of concentration, namely $p = 9.5 \times 10^{-2}$ mole%, the best overall agreement with the experimental line shape is obtained when the peak is located at 37.5 cm^{-1}, as shown in Fig. 8. Similar effects are observed for the Rb^+ and the Na^+ systems. The completely analogous deviation of the theoretical results from the experimental ones in the CsCl and CsI systems[12] suggests either that the alkali defects have been treated in a systematically wrong way, which is unlikely since they are thought to be rather well un-

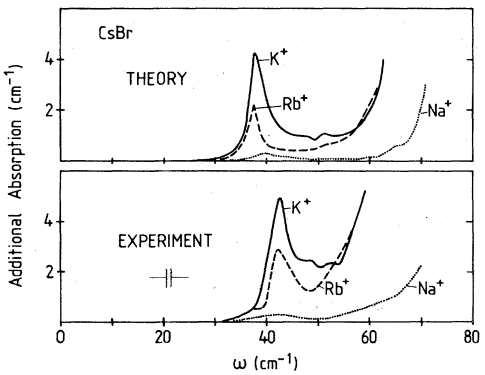

FIG. 8. Calculated and experimental (Ref. 2) infrared spectra for CsBr:Rb^+, CsBr:K^+, and CsBr:Na^+. Perturbed parameters correspond to those of model I given in Table IV.

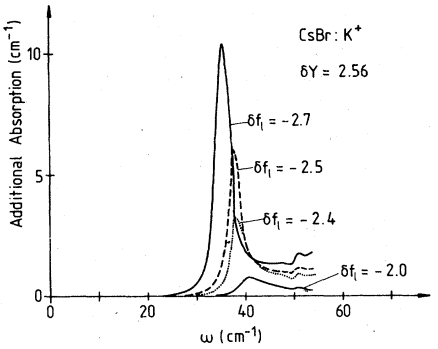

FIG. 9. Calculated infrared spectra of CsBr:K^+ for four different values of δf_l. The parameter $\delta\gamma$ is held constant to reproduce the ionic polarizability (Ref. 11) of K^+.

understood, or, rather, that the lattice dynamics contain inaccuracies common to all cesium halides.

To understand the above-mentioned discrepancy we have attempted to investigate the origin of these peaks. Since the peak position can be shifted continuously by changing δf_l, it is clear that these peaks do not arise from defect activated peaks in the host-crystal phonon density of states. It is, like the Tl^+ resonant band mode, a defect mode. In Fig. 10 is plotted the determinant $\|\underline{1}+\lambda\underline{g}_0\|$ as a function of frequency for all three systems. The parameters are chosen to match the spectra which are shown in Fig. 8.

The respective peak positions are indicated by arrows in the corresponding figures. The peaks are clearly not resonances, since their positions do not correspond to the resonance condition as given by Eq. (6). For the Rb^+ and K^+ systems, the peak positions coincide with a corresponding peak-like structure in the imaginary part of $\|\underline{1}+\lambda\underline{g}_0\|$. For CsBr:$Na^+$, the peak in the spectrum corresponds to a shoulder in the above-mentioned quantity. These structures in $\mathrm{Im}\|\underline{1}+\lambda\underline{g}_0\|$ can be shifted continuously in frequency by adjusting δf_l. As they shift towards higher frequencies they encounter maxima in both the real and imaginary parts of $\|\underline{1}+\lambda\underline{g}_0\|$, which correspond to maxima in the unperturbed Green's functions $\underline{g}_0$. Consequently the peaks in the calculated spectra get damped out at these frequencies. Hence the peaks in the calculated spectra occur at too low a frequency because the maxima in $\underline{g}_0$ occur at too low a frequency, which is a result of inaccuracies in the host-crystal phonons.

IV. CONCLUSIONS

For CsBr:Tl^+ we have shown that the only way to reproduce the experimental spectrum is by perturbing the displacements of the defect's second

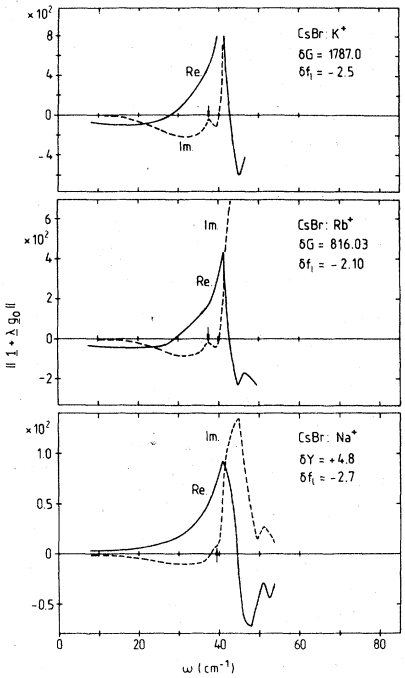

FIG. 10. Plot of $\|\underline{1}+\lambda\underline{g}_0\|$ as a function of frequency for CsBr:Rb^+, CsBr:K^+, and CsBr:Na^+.

neighbors. This could be achieved either by a direct coupling of the defect to these second neighbors, i.e., by δf_2, or by additionally perturbing the coupling between the first and the second neighbors of the defect, i.e., δf_s. Our best results are obtained for $\delta f_2 = 2.5$ and $\delta f_s = -0.2$. At this point it is not possible to state that the above values of the parameters truly represent the perturbed crystal, since a different combination of these two parameters can also reproduce the spectrum although perhaps not so well. We hope to resolve this uncertainty by investigating additional spectra, e.g., Raman spectra. Such calculations are now in progress and will be published at a later date.

Although the evidence that we have presented for the two parameters δf_2 and δf_s is strong indeed, the values which we have obtained for these are not what one would normally expect. For $\delta f_2 = 2.5$, and $\delta f_l = -3.02$, we have a situation in which the coupling of the defect to its second neighbor ($f_2 = 0 + \delta f_2 = 2.5$) is about as strong as the coupling to its nearest neighbors ($f_l = \frac{1}{2}A + \delta f_l = 2.6$), even though the model for the host crystal does not include any short-range coupling between second-nearest neighbors. This is a possible drawback for the host-crystal model. In Cs-halide crystals the distances from the nearest and second-nearest neighbors are almost the same; the ratio of the distances being $2/\sqrt{3} = 1.15$, which shows that the values of δf_l and δf_2 are not totally unreasonable.

Although the Tl^+ ion in thallous halides is smaller than the Cs^+ ion in cesium halides,[11] a negative value of δf_s indicates an outward relaxation around the defect. This, together with the strong coupling to second-nearest neighbors, seems to suggest that the Tl^+ defect in CsBr has a large extent, in which case the established picture of Tl^+ ion may break down. The amount of relaxation, however, is uncertain.

Finally, the infrared spectrum does not give sufficient information as to whether the polarizability of the Tl^+ defect is different from that of the Cs^+ ion. Also, the lack of precise knowledge of the relaxation around the defect adds to the uncertainty in the (volume-dependent) polarizability

For CsBr:Rb^+, CsBr:K^+, and CsBr:Na^+, we have found that the principal peaks result from defect modes rather than from defect-activated host-crystal phonons.

In all the systems that we have considered, polarization effects are seen to play an important role in determining the spectral line shapes even though the actual parameters δY and δG cannot be uniquely determined.

Except for the CsBr:Tl^+ RBM frequency, which is forced to agree with the experimental value, the peak positions in the calculated spectra are somewhat different from the observed ones for all four systems that we have considered. We believe that this is primarily a consequence of inaccuracies in the host crystal BSM phonons. Since the latter is not obtained by a fit to measured (neutron scattering) phonon dispersion curves, inaccuracies of this order are not unexpected.

The models that we have obtained for the perturbed systems should be valid for phonons of all symmetry types. However, the eventual test for this claim will be obtained from the results of the Raman calculations.

ACKNOWLEDGMENT

The authors are indebted to Professor U. Schröder who read the manuscript and made useful suggestions.

*Present address: The University of Nebraska-Lincoln, Behlen Laboratory of Physics, Lincoln, Nebraska 68588.

[1]L. Genzel, W. Prettl, and E. Siep, Opt. Commun. 1, 28 (1969).
[2]W. Prettl and E. Siep, Opt. Commun. 3, 407 (1971); in *Phonons*, edited by M. A. Nusimovici (Flammarion, Paris, 1971), p. 415.
[3]W. Prettl and E. Siep, Phys. Status Solidi 44, 759 (1971).
[4]J. B. Page, Jr., and D. Strauch, Phys. Status Solidi 24, 469 (1967).
[5]J. B. Page, Jr., Phys. Rev. B 10, 719 (1974).
[6]D. Strauch, Phys. Status Solidi 30, 495 (1968).
[7]P. N. Ram and B. K. Agrawal, Phys. Status Solidi 61, 341 (1974).
[8]T. Gethins, T. Timusk, and E. J. Woll, Jr., Phys. Rev. 157, 744 (1967).
[9]K. Dettmann and W. Ludwig, Phys. Kondens. Mater. 2, 241 (1964).
[10]G. Mahler and P. Engelhardt, Phys. Status Solidi 45, 543 (1971).
[11]J. R. Tessmann, A. H. Kahn, and W. Schockley, Phys. Rev. 112, 90 (1958).
[12]T. P. Martin, J. Phys. C 4, 2269 (1971).